JMEPEG (2024) 33:3787–3800
https://doi.org/10.1007/s11665-023-08871-9

1059-9495/$19.00

ORIGINAL RESEARCH ARTICLE

Multi-Objective Optimization for Turning Process of 304 Stainless Steel Based on Dung Beetle Optimizer-Back Propagation Neural Network and Improved Particle Swarm Optimization

Huan Xue, Tao Li, Jie Li, Yansong Zhang, Shiyao Huang, Yongchun Li, Chongwen Yang, and Wenqian Zhang

Submitted: 5 May 2023 / Revised: 5 September 2023 / Accepted: 8 October 2023 / Published online: 25 October 2023

Austenite stainless steel of type 304 is one of the most difficult materials to process. During the machining process, parts easily generate higher surface residual stress in cutting direction (CD) and production costs. To solve the problem, a multi-objective optimization method that combined Dung Beetle Optimizer-Back Propagation Neural Network (DBO-BPNN) and Improved Particle Swarm Optimization (IPSO) algorithm was adopted. Firstly, BPNN, Genetic Algorithm-Back Propagation Neural Network (GA-BPNN) and DBO-BPNN were established to map the nonlinear relationship between surface residual stress in CD and turning parameters. Secondly, a dataset of surface residual stress in CD and material removal rate under different turning parameters was obtained through finite element method (FEM) turning simulation. The dataset was applied into neural network to establish a nonlinear mapping relationship between turning parameters and surface residual stress in CD. The turning parameters are used as variables, the surface residual stress in CD and material removal rate are applied as objective functions. The optimal Pareto solution set of the surface residual stress in CD and material removal rate was acquired by combining DBO-BPNN and IPSO. Finally, turning experiments were designed to verify the accuracy of the turning simulation. The study shows that the surface residual stress in CD decreased by 38.47%, and the material removal rate increased by 91.69%.

Keywords 304 stainless steel, dung beetle optimizer algorithm, improved particle swarm optimization algorithm, multi-objective optimization, residual stress, turning process

1. Introduction

Austenite stainless steel of type 304 is one of the most widely used chromium-nickel stainless steels due to the excellent corrosion resistance (Ref 1). Surface residual stress is inevitably generated during material processing (Ref 2-4). The excessive residual stress will lead to corrosion and fatigue cracking of 304 stainless steel parts (Ref 5, 6), thus reducing the service life of the parts (Ref 7-10). Therefore, reducing residual stress is crucial to improving the service life of parts. Furthermore, the material removal rate is affected by turning speed, turning depth and feeds (Ref 11). Selecting suitable machining parameters will effectively decrease residual stress in parts and improve material removal rate, thus extending the service life of parts and reducing production costs (Ref 12).

The optimization of turning process parameters has been extensively studied. Mahdavinejad et al. (Ref 13) optimized the 304 stainless steel turning parameters. The optimized parameters decrease the surface roughness of 304 stainless steel parts and increase the tool service life. Years later, Taguchi-based gray correlation analysis was adopted by varghese (Ref 14) to optimize machining parameters. The optimization resulted in a reduction in cutting forces, surface roughness and chip reduction factor. In addition, numerous investigators have optimized turning parameters to improve productivity. Mirmohammadsadeghi et al. (Ref 15) used a non-dominated ranking genetic algorithm for multi-objective optimization of turning process parameters. Provide reliable reference turning process parameters for improving productivity. Zhou et al. (Ref 16) developed a genetic gradient boosting regression tree (GA-GBRT) algorithm to optimize the turning parameters. It enhanced turning efficiency. Su et al. (Ref 12) applied the Taguchi method to design turning experiments and developed a gray correlation degree regression model based on response

This invited article is part of a special topical issue of the Journal of Materials Engineering and Performance on Residual Stress Analysis: Measurement, Effects, and Control. The issue was organized by Rajan Bhambroo, Tenneco, Inc.; Lesley Frame, University of Connecticut; Andrew Payzant, Oak Ridge National Laboratory; and James Pineault, Proto Manufacturing on behalf of the ASM Residual Stress Technical Committee.

Huan Xue, Tao Li, Yansong Zhang, Shiyao Huang, Yongchun Li, and **Wenqian Zhang**, Hubei Key Laboratory of Modern Manufacturing Quality Engineering, School of Mechanical Engineering, Hubei University of Technology, Wuhan 430068, China; **Jie Li**, Hubei Guoan Special Steel Inspection and Testing Co. LTD, Huangshi 435000, China; **Chongwen Yang**, School of Mechanical Science and Engineering, Huazhong University of Science and Technology, Wuhan 430076, China. Contact e-mail: wenqian_zh@hust.edu.cn.

surface methodology(RSM). The optimization method achieved a trade-off between cutting quality, productivity, and energy consumption. Alajmi et al. (Ref 17) proposed a machine learning method using an Adaptive Neuro-Fuzzy Inference System-Quantum Particle Swarm Optimization Algorithm (ANFIS-QPSO) to predict turning surface roughness values of AISI 304 stainless steel. The results show the method can ensure high accuracy in predicting the surface roughness values of the turning process. However, little research has been studied on optimizing turning parameters (especially tool parameters) to achieve both minimum residual stress and maximum material removal rate.

Numerous investigators have combined neural networks and particle swarm optimization algorithms (PSO) and applied them to the optimization of machining parameters. Jafarian et al. (Ref 18) optimized the surface roughness, tool life, and cutting force in the turning process using artificial neural network and PSO algorithm. The combination of GA and PSO provides a more accurate prediction of the effect of each parameter on tool life, surface roughness and cutting forces. Later, a new PSO algorithm was proposed by Wang (Ref 19) to solve mixed-variable optimization problems (MVOP), which can handle both continuous and discrete decision variables. The overall efficiency of the system was enhanced. Mohammadi et al. (Ref 20) optimized the parameters of the arc welding process using a PSO algorithm to reduce the tensile residual stress in 304 stainless steel butt-welded plates with 4-15 mm thicknesses. Zhou et al. (Ref 21) optimized the process parameters for marine diesel engine block hole system machining employing an IPSO algorithm, which improved the diesel engine's operational efficiency. The combination of rough set and PSO algorithm was employed to distinguish images by Zhang (Ref 22). The algorithm enhanced the sharpness of image edges, enriched the texture details of the image, and preserved the information in the smooth areas of the image. Moreover, several investigators have studied the welding process. Moghaddam et al. (Ref 23) took the heat-affected zone and weld geometry as targets to optimize the machining parameters and joint geometry by applying an artificial neural network and PSO algorithm. The optimal process parameters reduce the energy consumption by 11.4% and increase weld bead integrity as well as tensile strength by 9.07 and 1.48%, respectively. Kahhal et al. (Ref 24) performed a multi-objective optimization of the mechanical properties of AH12 1050 aluminum alloy friction-stir-welding by combining the response surface method with a multi-objective PSO algorithm. The method improved the material's strength and hardness. However, few studies have applied neural networks and PSO to optimize turning parameters, especially tool parameters, while aiming for the minimum residual stress and maximum material removal rate.

The metal turning process is more complex, with high temperature, large deformation, large strain rate and other complex factors. Residual stress has an impact on the service life and material removal rate affects production costs. Optimizing the turning parameters is vital to reduce residual stress and increase material removal rate. Reasonable turning parameters can reduce the surface residual stress of parts, improve material removal rate, thereby reducing production costs and extending the service life of parts. Production costs are affected by production efficiency, and production efficiency and residual stress are affected by turning parameters (Ref 25-27). Turning speed and turning depth have a significant impact on surface residual stress and production efficiency. Although some research has been conducted to optimize turning speed, turning depth, and feed rate for machining quality and production cost of turning 304 stainless steels, there has been less emphasis on simultaneously optimizing turning speed, turning depth, tool rake angle, tool relief angle, and turning edge radius. Therefore, this paper proposes a multi-objective optimization method that combines DBO-BPNN and IPSO to optimize the above parameters simultaneously to achieve the dual objectives of minimizing surface residual stress and maximizing material removal rate. The dung beetle optimization algorithm (DBO) (Ref 28) has the advantages of fast convergence speed and high prediction accuracy than others. Combining with back-propagation neural network (BPNN), it can effectively establish the nonlinear mapping relationship between turning process parameters and surface residual stress. The improved particle swarm optimization (IPSO) algorithm can realize the multi-objective optimization problem effectively.

2. Multi-objective Optimization Model

2.1 Mathematical Model of Multi-Objective Optimization

The surface residual stress in CD and material removal rate of turning 304 stainless steels were used as the objectives to optimize the turning parameters. The mathematical model of the optimization problem is shown in Eq 1. Equation 2 represents the material removal rate.

$$\begin{cases} H = [v, h, e, f, r] \\ f_1(H) = \min(R_1(H)) \\ f_2(H) = \max(R_2(H)) \\ H \in \Omega \end{cases} \quad \text{(Eq 1)}$$

$$R_2(H) = v \times h \times 10^{-3} \quad \text{(Eq 2)}$$

where $H = [v, h, e, f, r]$ represents the turning parameter, v, h, e, f and r denote the turning speed, turning depth, tool front angle, tool back angle and tool radius, respectively. The feasible domain set Ω indicates the settable parameters of the turning process; $R_1(H)$ and $R_2(H)$ are the surface residual stress in CD and material removal rate under the condition of turning parameter H, respectively. The objective functions are both f_1 and f_2.

2.2 Neural Network

2.2.1 BPNN. Finite element method (FEM) of turning simulation is time-consuming and laborious to obtain surface residual stress in CD under different turning parameters. This paper applies BPNN to predict the residual stress of 304 stainless steel under different turning parameters.

Traditional BPNN takes a long time to train with the slow convergence speed. The BPNN is sensitive to the initial weights and thresholds and may get trapped in locally optimal solutions (Ref 29). Therefore, an optimization algorithm is needed to optimize the weights and thresholds of BPNN to avoid falling into a locally optimal solution.

2.2.2 GA-BPNN. Since the traditional BPNN is more sensitive to the initial weights and thresholds, and easily falls into local optimal solutions. In this paper, genetic algorithm (GA) is adopted to optimize the BPNN. GA is an optimization

algorithm inspired by natural selection (Ref 30), which selects the optimal individual based on the concept of survival of the fittest. After selection, crossover and mutation operations, the fitness of each individual was calculated, those with higher fitness will be retained and those with lower fitness will be removed. Repeat above operation until the maximum number of iterations was reached. Equation 3, 4 and 5 are selection, crossover and mutation operations, respectively. The surviving individuals will be used as the new initial weights and thresholds for BPNN.

$$p_i = \frac{k/F_i}{\sum_{j=1}^{n} f_i} \quad \text{(Eq 3)}$$

In Eq 3, F_i means the fitness value of individual i, $k = 10$ denotes the coefficient, and p_i is the probability that individual i is selected.

$$\begin{cases} a_{\mathrm{kj}} = a_{\mathrm{kj}}(1-b) + a_{\mathrm{lj}} b \\ a_{\mathrm{lj}} = a_{\mathrm{lj}}(1-b) + a_{\mathrm{kj}} b \end{cases} \quad \text{(Eq 4)}$$

where a_k represents the k th chromosome, a_{kj} indicates the crossover operation of the k th chromosome and the l th chromosome at the j th position.

$$a_{\mathrm{lj}} = \begin{cases} a_{\mathrm{ij}}\left(a_{\mathrm{ij}} - a_{\max}\right) * r_0(1 - g/G_{\max}), r > 0.5 \\ a_{\mathrm{ij}}\left(a_{\min} - a_{\mathrm{ij}}\right) * r_0(1 - g/G_{\max}), r \le 0.5 \end{cases} \quad \text{(Eq 5)}$$

Where $a_{\max}$ and $a_{\min}$ denote the upper and lower bounds of gene a_{ij}, r_0 is a random number, g means the current iteration number, G indicates the maximum iteration number, and r represents a random number between 0 and 1.

2.2.3 DBO-BPNN. Although the GA-BPNN avoids getting into local optimal solutions, the global search capability of GA-BPNN is insufficient to search for the global set of optimal solutions. Therefore, this paper also employs DBO with better global search capability to optimize BPNN. Xue et al (Ref 28) inspired by the ball-rolling, dancing, foraging, stealing, and reproduction behaviors of dung beetles, a dung beetle optimization algorithm was developed. The DBO algorithm divides the initial population into four sub-populations to search for the optimal position respectively. The global optimal position was obtained by comparing each subpopulation. The solutions for the optimal position of the dung beetle were the weights and thresholds of BPNN. DBO was adopted to optimize the weights and thresholds of BPNN to improve its convergence speed and reduce train time, while also getting the best global solution in global search. The distribution of each subpopulation is shown in Table 1. The initial population was thirty.

Circle Chaos Mapping was added to the initialized populations to make each population globally uniform distributed.

$$x_i(t+1) = x_i(t) + a_0 - \mathrm{mod}\left(\frac{b_0}{2\pi}\sin 2(\pi x_i(t)), 1\right) \quad \text{(Eq 6)}$$

The position of the ball-rolling dung beetle is updated in the follows:

No-obstacles:

$$x_i(t+1) = x_i(t) + a \times k \times x_i(t-1) + b \times |x_i(t) - X^w| \quad \text{(Eq 7)}$$

Obstacles:

$$x_i(t+1) = x_i(t) + \tan\beta |x_i(t) - X^w| \quad \text{(Eq 8)}$$

where t indicates the current number of iterations and $x_i(t)$ denotes the position of the i th dung beetle at t th iterations. $a_0 = 5, b_0 = 0.2$. $k \in (0, 0.2]$ represents the constant of the bias coefficient and $b \in (0, 1)$ is a constant. $a = -1$ *or* 1 is a natural coefficient and X^w refers to the global worst position. $\beta \in (0, \pi]$, when $\beta = 0, \pi/2, \pi$, the position of the dung beetle remained unchanged. Please refer to Ref. 28 for other subpopulation position update methods.

The process of DBO to search for the best solution is shown in Fig. 1.

In order to avoid fall into a partial optimum solution, the formula for the difference of square was incorporated with Equation 7 and 8:

$$x_i(t+1) = x_i(t) + a \times k \times x_i(t-1) + b \times \left|(x_i(t))^2 - (X^w)^2\right| \quad \text{(Eq 9)}$$

$$x_i(t+1) = x_i(t) + \tan\beta \left|(x_i(t))^2 - (X^w)^2\right| \quad \text{(Eq 10)}$$

2.3 IPSO Algorithm and Optimization Process

The particle swarm algorithm multi-objective optimization process is shown in Fig. 2. The position of each particle represents a turning process parameter. The particle searchable range was set and an initial particle group position was randomly generated based on the relationship between surface residual stress in CD and turning parameters. Then, the fitness of each particle was calculated. The Pareto inter-dominance relationship between particles indicates whether each particle was a non-dominated solution and selected the global optimal particle. If a particle's position and velocity were beyond the search range, the boundary position was in placed by this particle, and its velocity was reversed. Superior solutions were searched in updated particles and saved to the Pareto frontier solution set. The distance between particles was calculated in the solution set; the excess particles were randomly removed when either maximum number of particles or maximum distance limit was reached. Repeated this process until reaching maximum number of iterations, then gained best set of Pareto solutions for turning 304 stainless steel process parameters.

The update of velocity and position of the t th iteration of the i th particle is shown in Eq 11 and 12 respectively:

Table 1 The quantity of each subpopulation of dung beetle

Subpopulation	Ball-rolling dung beetle	Breeding dung beetle	Foraging dung beetle	Thief dung beetle
Quantity	6	6	7	11

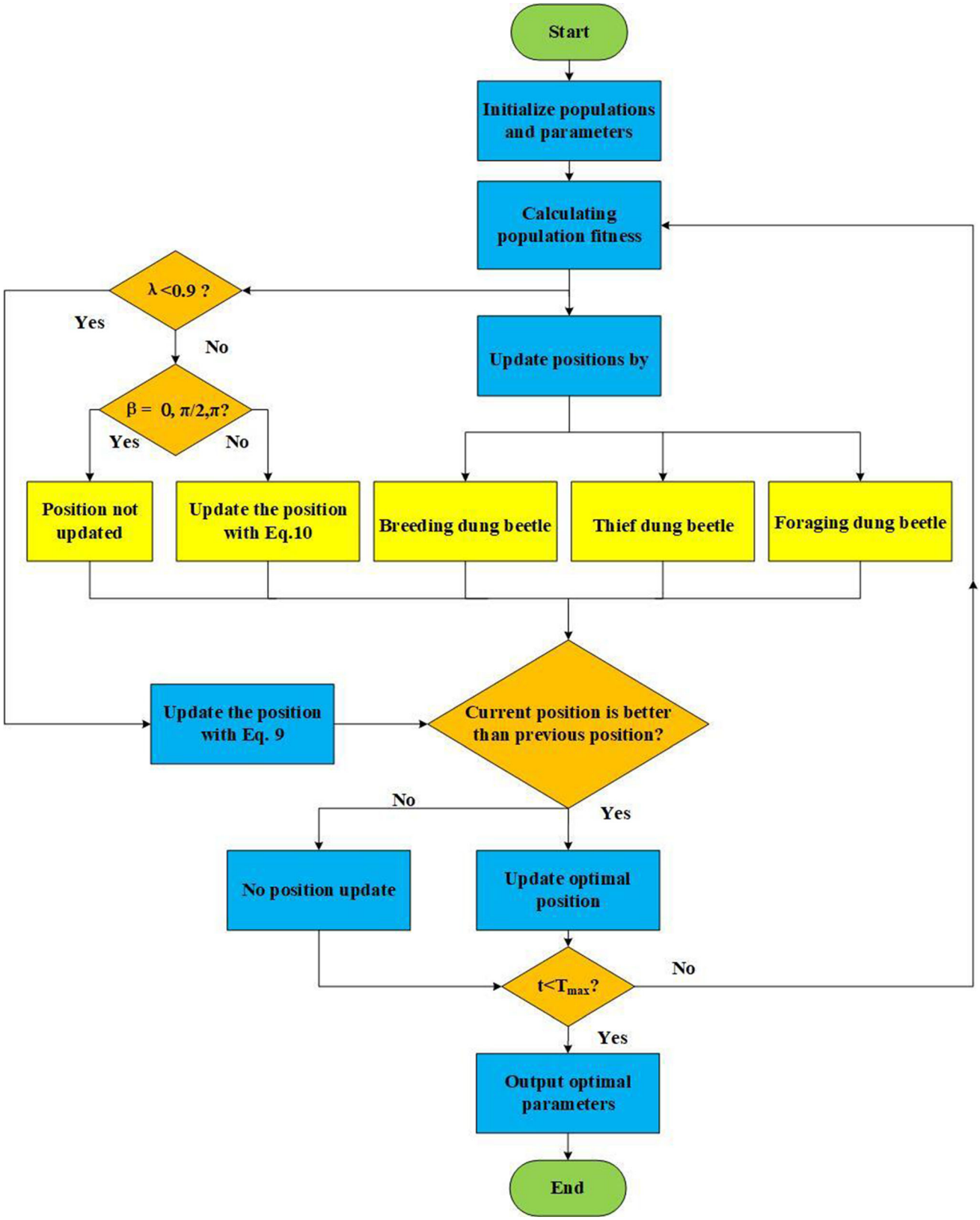

Fig. 1 DBO Optimization Process

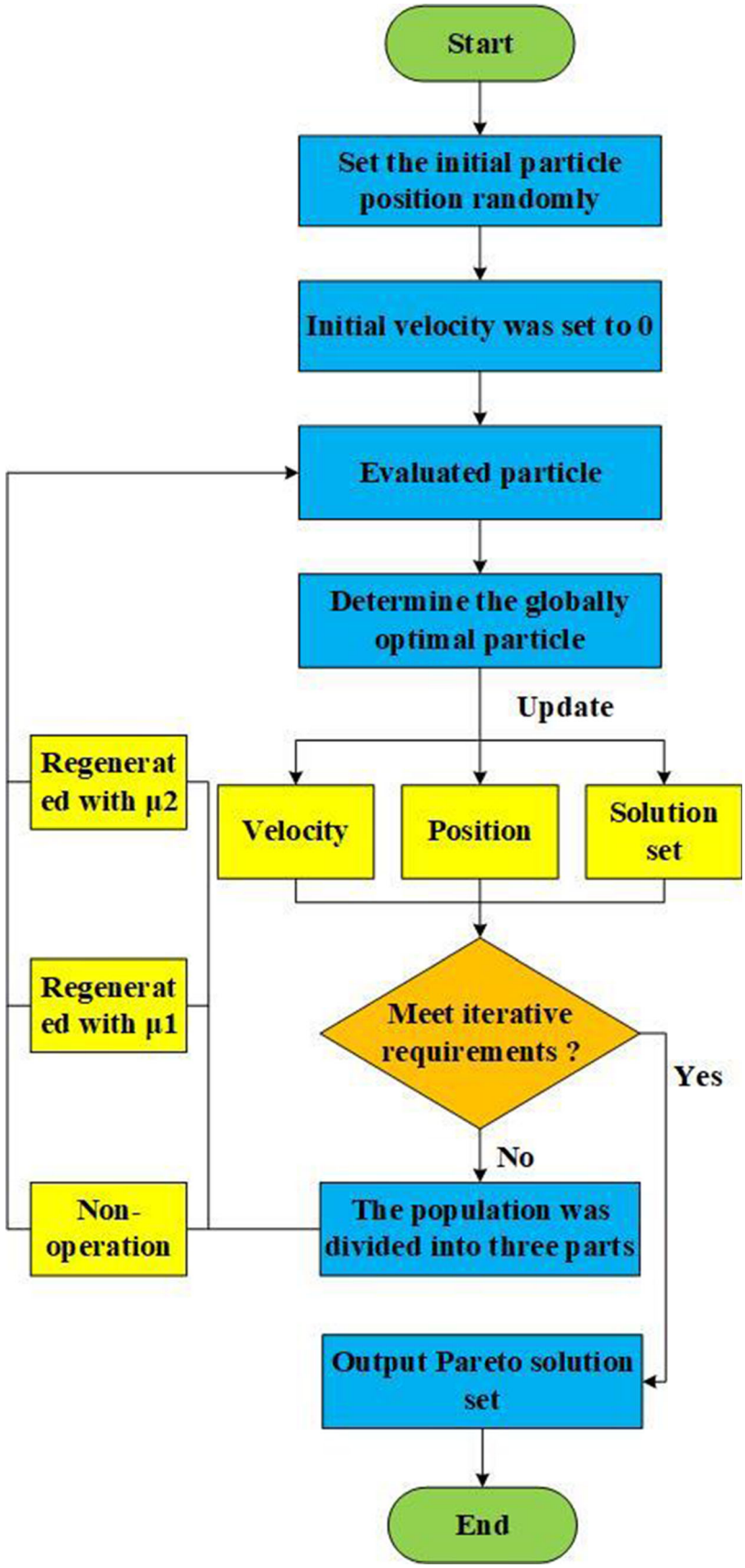

Fig. 2 IPSO optimizes flowchart

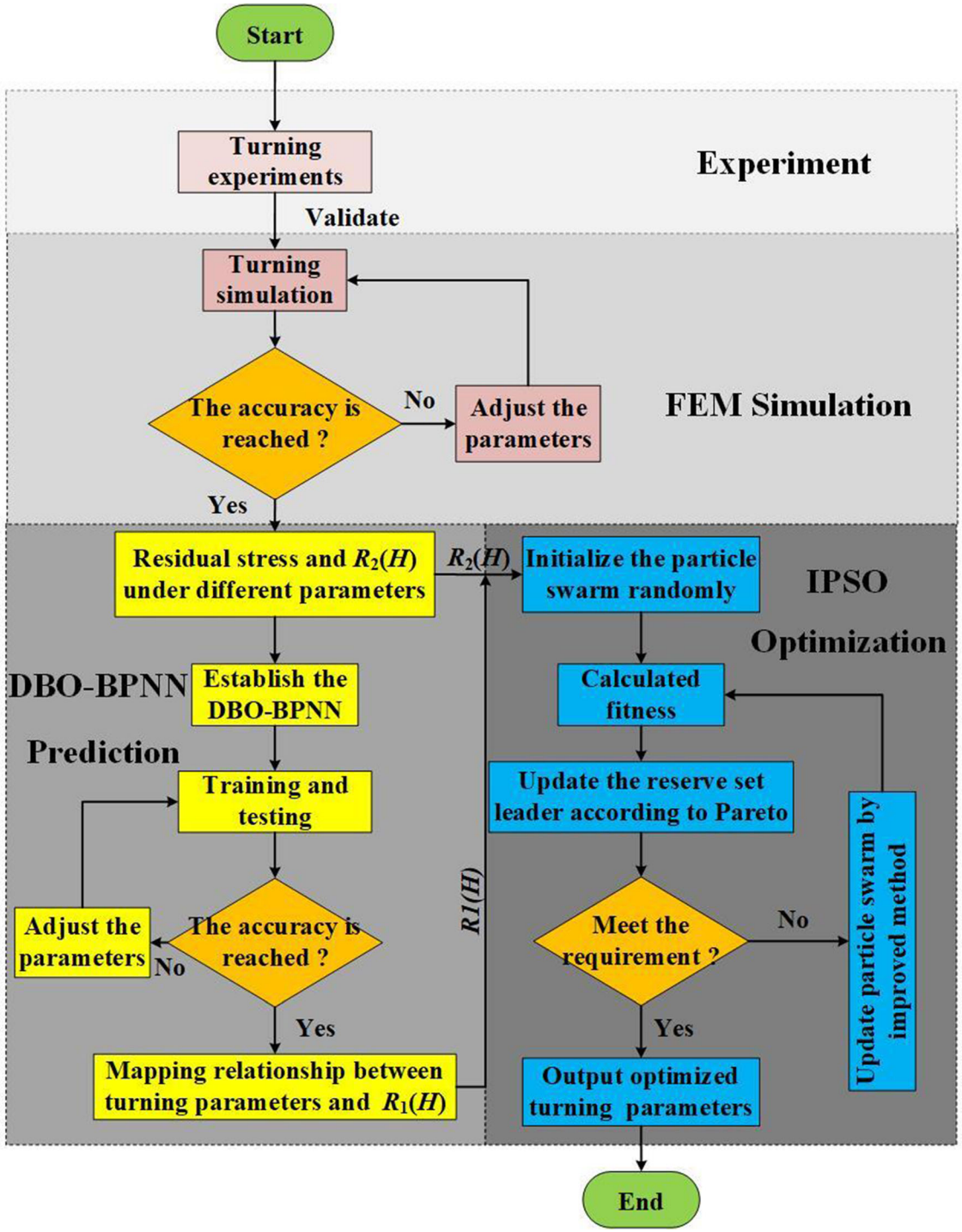

Fig. 3 Overall optimization solution process

Table 2 Chemical element composition of 304 stainless steel (mass fraction/%)

C	Si	P	Mo	Mn	Cr	Ni	Fe
0.0389	0.446	0.0225	0.172	0.675	18.3	8.53	Balance

$$v_i(t+1) = \omega v_i(t) + c_1 r_1(t)[G_i(t) - g_i(t)] + c_2 r_2(t)\left[G_g(t) - g_i(t)\right] \quad \text{(Eq 11)}$$

$$g_i(t+1) = g_i(t) + v_i(t+1) \quad \text{(Eq 12)}$$

In Eq 11, ω means the inertial weight coefficient, $\omega = 0.4$; $v_i(t)$ and $g_i(t)$ denote the velocities and positions of the i th particle at the t th iteration, respectively; c_1 and c_2 represent

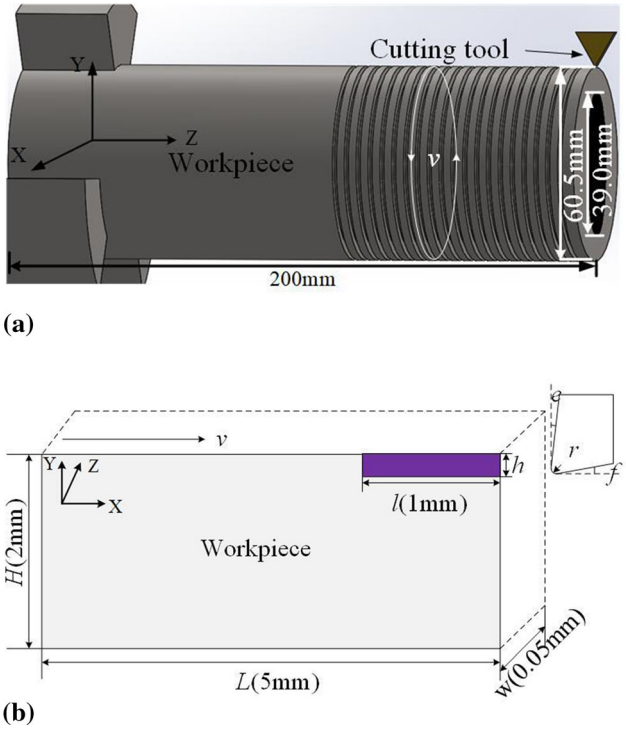

Fig. 4 Turning experiment and simulation model (L and H are the length and height of the simulation model. v, h, e, f, r, w and l mean the turning speed, turning depth, tool front angle, tool back angle, tool radius, turning width and turning length, respectively) (a) 3D experimental turning model, (b) 2D simulation model

particle acceleration constants, and the value is $c_1 = c_2 = 2$; $r_1(t)$ and $r_2(t)$ indicate two independent random numbers of the t th iteration; $G_i(t)$ refers to the historical optimal position of the i th particle at the t th iteration; $G_g(t)$ is the optimal position of all particles at the t th iteration.

In the iterative process, the particle swarm was divided into three parts. Part 1 iterated according to the particle swarm optimization algorithm. Part 2 set random initial population probability $\mu_1 = 0.5$ and regenerated particles randomly in each iteration with a probability of μ_1 to make them globally distributed and avoid falling into local optimal solutions. With an increase in iterations, the range of optimal solution sets of Pareto frontier had been found to a large extent. The convergence should be within the range of optimal solutions to get the best Pareto frontier. In Part 3, particles in population were randomly regenerated with probability μ_2 during each iteration where μ_2 decreased with an increase in iterations as shown in Eq 13.

$$\mu_2 = e^{-\sqrt{\frac{t}{T_{\max}}}} \quad \text{(Eq 13)}$$

In Eq 13, t represents the current number of iterations, $T_{\max}$ indicates the maximum number of iterations.

BPNN was established to map the relationship between the turning process parameters and surface residual stress in CD with the turning parameters as input and surface residual stress in CD as output. Then DBO and GA were employed to optimize BPNN, respectively. Optimized BPNN for predicting surface residual stress in CD of 304 stainless steel. Taking $R_1(H)$ and $R_2(H)$ as fitness functions of IPSO, turning parameters were optimized to get minimum surface residual stress in CD and maximum material removal rate. In this paper, optimal solution set of best turning parameters was obtained

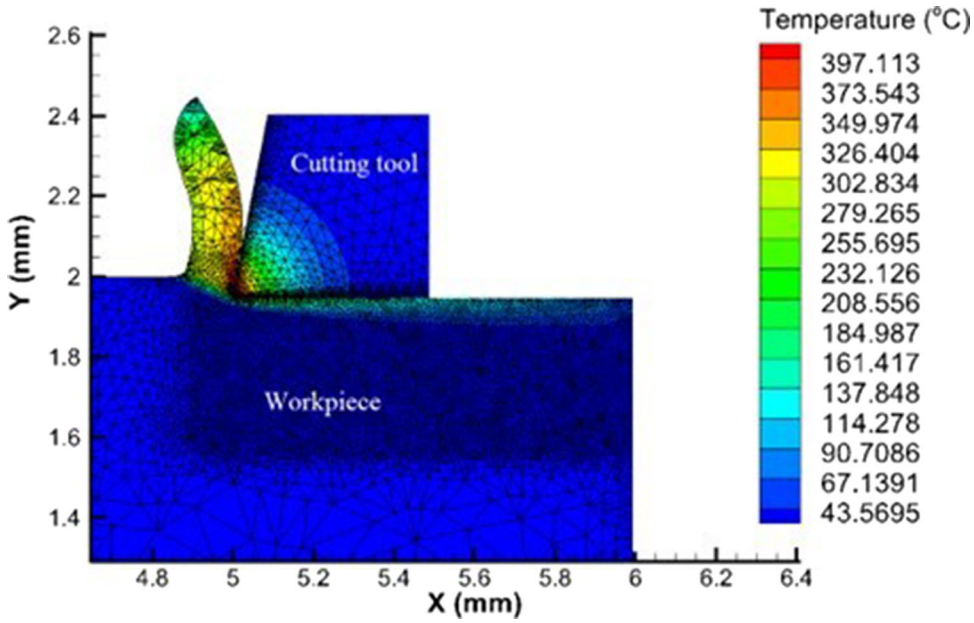

Fig. 5 Finite element chip formation process (turning speed v = 200 m/min, turning depth h = 0.05 mm, tool front angle e = 11°, tool back angle f = 0° and tool radius r = 0.02 mm)

Table 3 304 stainless steel material physical performance parameter

Density, kg/m^3	Young modulus , GPa	Poisson ratio	Heat conductivity, W/(m × K)	thermal diffusion coefficient, 1/K	specific heat, J/(kg × K)
7930	193	0.28	16.2	16×10^{-6}	500

Table 4 304 stainless steel J-C model parameters

Parameter	*A*, MPa	*B*, MPa	*C*	*n*	*m*	T_{room}, °C	T_{melt}, °C
Value	452	694	0.0067	0.331	0.996	20	1400

Table 5 Parameter variation range for turning simulation

Turning parameters	Turning speed *v*, m/min	Turning depth *h*, mm	Tool front angle *e*, °	Tool back angle *f*.°	Tool radius *r*, mm
Variation range	50 ~ 300	0.05 ~ 0.30	-11 ~ 11	0 ~ 11	0.02 ~ 0.04

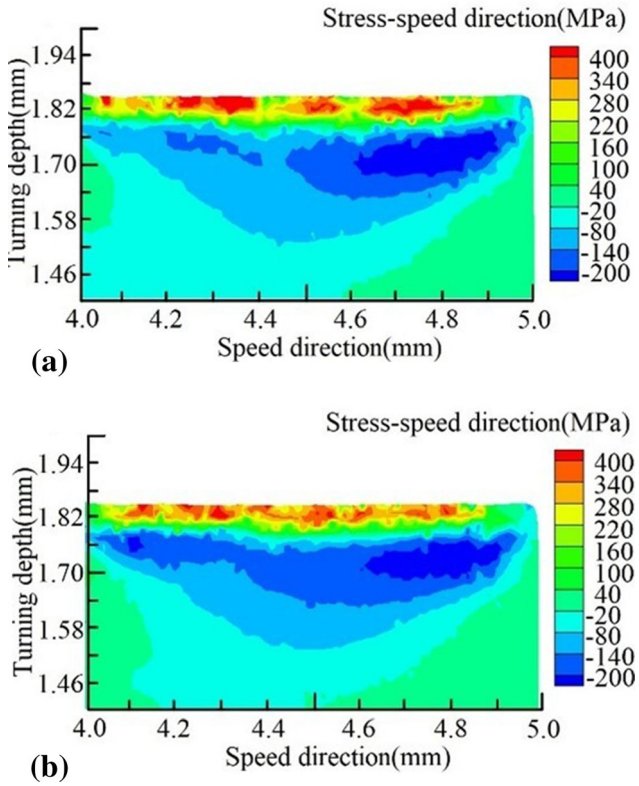

Fig. 6 Simulation residual stress in turning speed direction distribution (turning depth $h = 0.15$ mm, tool front angle $e = 11°$, tool back angle $f = 0°$ and tool radius $r = 0.04$ mm) (a) Turning speed 100 m/min, (b) Turning speed 200 m/min

applying Pareto mutual dominance relationship. The overall optimization solution process is shown in Fig. 3.

In this paper, the optimization scheme is settled as follows:

- Step 1: A uniform design method was adopted to acquire the turning parameters within the parameters of turning. A turning simulation model was built and the reliability of the turning simulation was verified by using turning experiments. Turning surface residual stress in CD under different turning parameters were obtained by FEM simulation. It was divided into a neural network training data set and a test set.
- Step 2: The neural network model was built with the turning parameters as input and the surface residual stress in CD as output. The test set was substituted into the trained neural network model. The neural network parameters were adjusted to bring the prediction error to the specified accuracy.
- Step 3: By encoding the turning parameters, the initialized particle population was randomly generated. Each individual's velocities and positions were calculated using Equation 11 and 12.
- Step 4: The set of non-dominated solutions was obtained adopting the Pareto dominance relation. If there was a dominant solution, or the number of particles was maximized. Updated the set of non-dominated solutions.
- Step 5: Select the particles in the non-dominant solution set as the leader randomly. According to the improved

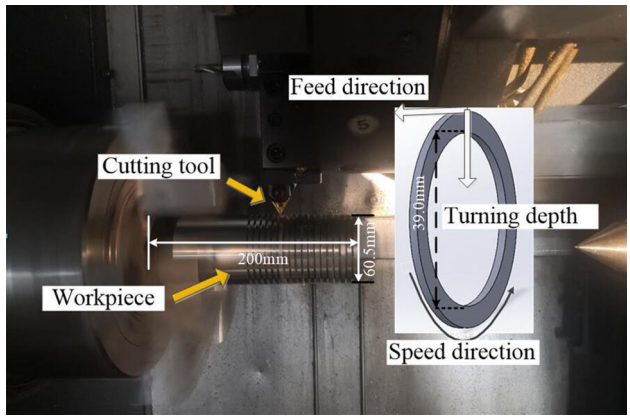

Fig. 7 Experimental processing of 304 stainless steel turning

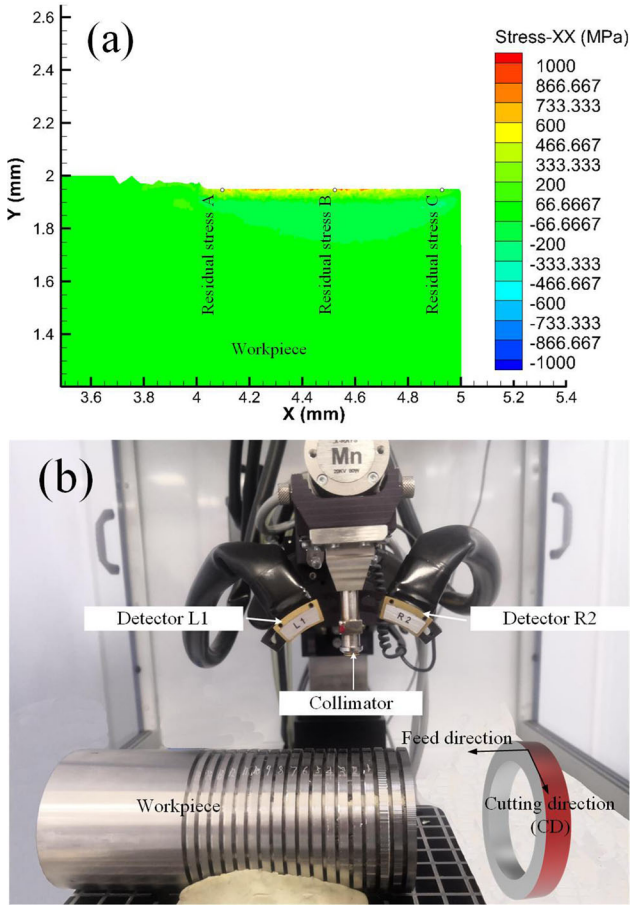

Fig. 8 Measurement of surface residual stress in CD (a) Measurement of surface residual stress in CD in turning simulation, (b) Measurement of surface residual stress in CD in turning experiment

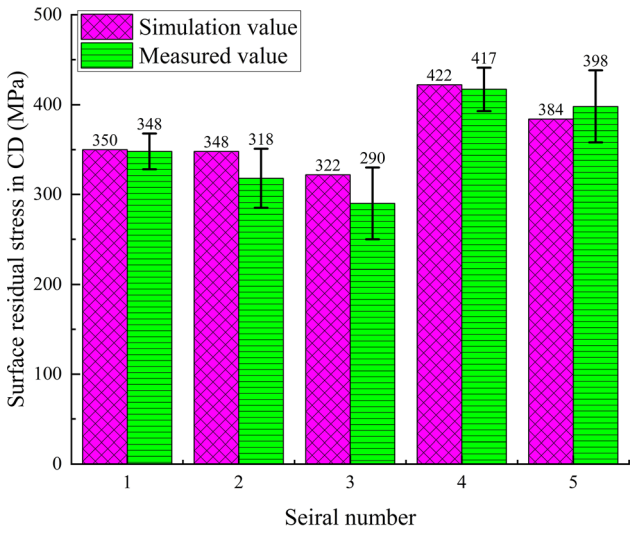

Fig. 9 Simulated and measured value of 304 stainless steel surface residual stress in CD

algorithm, the position and velocity of the particle swarm were updated.

- Step 6: The Pareto frontier solution set will be output as the iteration count reaches the maximum.

When multiple targets were optimized at the same time, different weight coefficients can be set for optimization targets through Eq 14. Convert multi-objective optimization to single-objective optimization.

$$\begin{cases} G = \sum_{j=1}^{k} a_j f_j \\ \sum_{j=1}^{k} a_j = 1 \end{cases} \quad \text{(Eq 14)}$$

In Eq 14, $k = 2$, $0 \le \alpha_1 \le 1$, $0 \le \alpha_2 \le 1$. $\alpha_1 = 1$, output the optimal solution of minimum residual stress; $\alpha_2 = 1$, output the optimal solution of maximum material removal rate; $\alpha_1 = \alpha_2 = 0.5$, output the optimal solution of minimum surface residual stress in CD and maximum material removal rate at the same time.

3. Materials and Method

3.1 Material

The sample was made of 304 stainless steel tube. The inner ring diameter and outer ring diameter was 39.0 mm and 60.5 mm respectively. The workpiece was subjected to solution heat treatment and stress relief heat treatment before turning. The chemical composition of the material is listed in Table 2.

3.2 Turning Simulation

The finite element method (FEM) model for 304 stainless steel was established by AdvantEdge^{TM}. Fig. 4(a) and (b) are the 3D experimental turning model and 2D simulation model of the FEM of turning, respectively. The X, Y and Z directions correspond to speed direction, turning depth and feed direction. The initial temperature was set to 20 °C, and the friction coefficient was 0.3.

Figure 5 represents the FEM of chipping. During the turning process, the highest temperature was 397 °C at the turning tool. The surface residual stress in CD after machining was 177 MPa. Table 3 shows the physical property parameters of 304 stainless steel materials (Ref 31). Johnson-Cook(J-C) model was used to describe the constitutive relationship of metal during turning simulation. The expression of the J-C criterion is shown in Eq 15.

$$\sigma(\varepsilon, \dot{\varepsilon}, T) = (A + B\varepsilon^n)\left(1 + C\ln\frac{\dot{\varepsilon}}{\varepsilon_0}\right)\left(1 - \left(\frac{T - T_{\text{room}}}{T_{\text{melt}} - T_{\text{room}}}\right)^m\right) \quad \text{(Eq 15)}$$

Where σ denotes the flow stress; ε means equivalent plastic strain; $\dot{\varepsilon}$ indicates the equivalent shaping strain rate; ε_0 represents the reference strain rate; A means the initial yield stress; B is the strain strengthening parameter; C indicates the strengthening parameter dependent on the strain rate; n and m are the work hardening index and thermal softening coefficient, respectively; T_{room} and T_{melt} refer to the room temperature and the melting temperature of the material, respectively. J-C model parameters of 304 stainless steel (Ref 31) workpieces are shown in Table 4.

Table 6 Different turning parameters

Serial number	Turning speed *v*, m/min	Turning depth *h*, mm	Tool front angle *e*, °	Tool back angle *f*, °	Tool radius *r*, mm
1	150	0.10	11	0	0.04
2	100	0.15	11	0	0.04
3	200	0.15	11	0	0.04
4	150	0.15	11	0	0.04
5	150	0.20	11	0	0.04

Table 7 The data sets of the residual stress in CD for Turning 304 stainless steel

serial number	Turning speed *v*, m/min	Turning depth *h*, mm	Tool front angle *e*, °	Tool back angle *f*, °	Tool radius *r*, mm	Residual stress $R_1(H)$, MPa
1	150	0.2	11	0	0.04	384
2	200	0.15	7	0	0.04	430.4
3	200	0.05	11	0	0.04	528.23
4	200	0.1	11	0	0.04	367.34
5	200	0.15	11	0	0.04	322.4
…	…	…	…	…	…	…
134	200	0.15	11	9	0.03	265.75

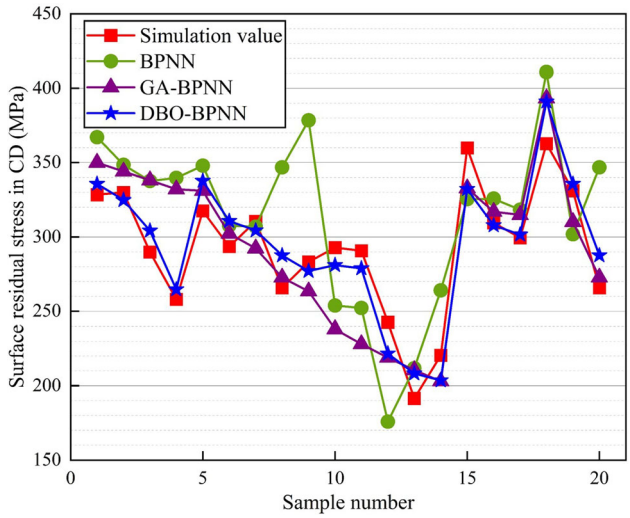

Fig. 10 Predicted values of the surface residual stress in CD in three different prediction models

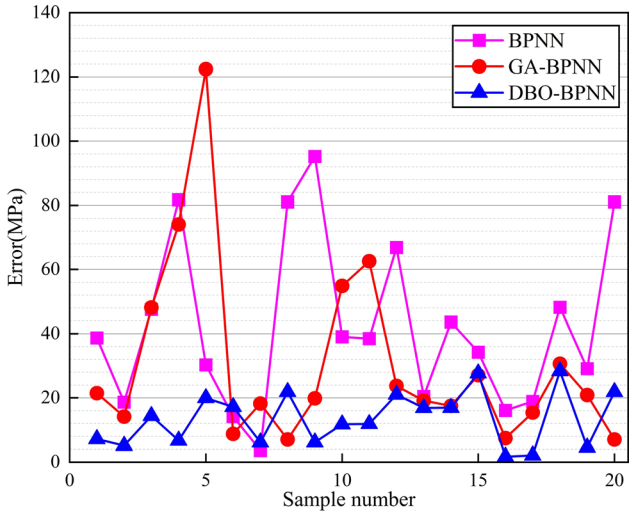

Fig. 11 Error of the three different prediction models

In the simulation experiment of turning 304 stainless steels, the range of turning parameters changes as shown in Table 5.

In the turning simulation, Figs. 6(a) and (b) show the residual stress distribution in the turning speed direction at turning speeds of 100 m/min and 200 m/min, respectively. The residual stress in the speed direction shows a trend of decreasing first and then increasing with the increase of depth. The minimum residual stress is about 0.10 ~ 0.15 mm below the surface and reaches − 200 MPa. The machined surface is mainly tensile residual stress.

3.3 Experiment Validation

Turning experiments were conducted to verify the reliability of the turning simulation. The lathe used for experimental processing was HTC2050 NC, and the turning tool was TNMG160408-MM. The turning experiment process is shown in Fig 7. The 304 stainless steel blank was machined by cutting. The groove depth and width were 5 and 2 mm respectively. A 3 mm wide annular specimen was obtained and then the annular surface was turned.

Proto iXRD was used to measure the residual stress on the surface of the specimen. The target material is manganese target. The working voltage and current were 20 KV and 4 mA, respectively. Analyzing the diffraction peak corresponding to the austenite {3,1,1} crystal plane, its 2θ angle was about 152°. After turning experiment, residual stress measurements in the direction of turning speed on the surface of each specimen were conducted three times, providing the surface residual stress in CD values of the workpiece after the experiment. After turning simulation, three residual stress values (Residual stress A, Residual stress B and Residual stress C) of turning speed direction (X direction) were taken at the positions of 10, 50,

Table 8 Turning parameters of 20 rows test sets

Serial number	Turning speed *v*, m/min	Turning depth *h*, mm	Tool front angle *e*, °	Tool back angle *f*, °	Tool radius *r*, mm
1	200	0.15	11	5	0.04
2	50	0.15	11	0	0.04
3	100	0.15	11	0	0.04
4	200	0.2	11	0	0.04
5	250	0.15	11	0	0.04
6	300	0.15	11	0	0.04
7	50	0.15	11	0	0.03
8	100	0.15	11	0	0.03
9	150	0.15	11	0	0.03
10	300	0.15	11	0	0.03
11	50	0.15	11	0	0.02
12	100	0.15	11	0	0.02
13	150	0.15	11	0	0.02
14	250	0.15	11	0	0.02
15	300	0.15	11	0	0.02
16	200	0.15	11	0	0.03
17	150	0.15	11	0	0.03
18	200	0.15	-3	0	0.04
19	200	0.15	-3	0	0.02
20	200	0.15	11	9	0.03

Table 9 Parameter variation range for optimization

Turning parameters	Turning speed *v*, m/min	Turning depth *h*, mm)	Tool front angle *e*, °	Tool back angle *f*, °	Tool radius *r*, mm
Variation range	30 ~ 400	0.02 ~ 0.40	-15 ~ 15	0 ~ 15	0.02 ~ 0.06

and 90% within the machined region. The average value of these three residual stresses was considered as the surface residual stress in CD of the turning simulation. In turning simulation, XX direction corresponds to the CD of the workpiece in turning experiment. The measurement process is illustrated in Figure 8.

4. Results and Discussion

4.1 Residual Stress

The simulated and measured values of machined direction surface residual stress in CD of workpiece corresponding to different turning parameters are shown in Fig. 9, with a maximum error of 32 MPa. The experiment numbers in Figure 9 correspond to the serial number in Table 6. Under different turning parameters, the mean absolute percentage error of residual stress between simulated and measured is 5.10%. These results demonstrate that the surface residual stress in CD measured by simulation and experiment have good agreement, and the established turning model accurately predicts surface residual stress in CD. Different turning parameters are shown in Table 6.

The surface residual stress in CD data under different turning parameters were obtained by the FEM simulation. Table 7 shows the data sets (the complete dataset is available in the supplementary file) required by the neural network prediction model. The first five columns are input and the last column is output. The range of variation for turning speed was 50 to 300 m/min, the range of variation for turning depth was 0.05 to 0.30 mm, the range of front angle for the tool was − 11° to 11°, the range of back angle for the tool was 0° to 11°, and the range for the tool radius was 0.02 to 0.04 mm.

The average absolute error of the forecast was set within 5%. The structure and parameters of the neural network were adjusted, with the number of hidden layers being 3 and the number of hidden layer nodes being 15, 20, and 15. The transfer function from the input layer into the hidden layer was the ''hyperbolic tangent function'', while the other transfer functions were ''linear functions''. The maximum number of iterations was 1000. The additional energy factor was 0.95, the minimum energy gradient was 0.01, and the learning rate was 0.0008.

The data set consisted of 134 data sets that were scrambled, with the first 114 rows of the data set serving as the training set and the last 20 rows serving as the test set. The BPNN and GA-BPNN models used the same setup. Figure 10 shows the predicted values of three different prediction models. Figure 11 shows the error of three prediction models. Table 8 represents the turning parameters of 20 rows test sets.

The turning parameters for each group in Fig. 10 and 11 are provided in Table 8. The maximum prediction errors of surface residual stress in CD for BPNN, GA-BPNN and DBO-BPNN were 95 MPa, 122 MPa, and 28 MPa, respectively. The mean absolute percentage errors of BPNN, GA-BPNN and DBO-BPNN predictions were 15.17, 10.68 and 4.77%, respectively. The prediction error of DBO-BPNN was minimum. In this paper, DBO-BPNN was found to be the best choice for predicting surface residual stress in CD. It can map the

relationship between surface residual stress in CD and turning parameters well.

4.2 Turning Parameters and Material Removal Rate

When optimizing the process parameters of 304 stainless steel, the range of tuning parameters should be constrained. The changing range of turning parameters is shown in Table 9. The DBO-BPNN has been employed as the fitness function of IPSO as a result of this model can accurately represent the relationship between the turning parameters and the surface residual stress in CD. Through the debugging algorithm, the particle population size was determined to be 240, the maximum number of iterations was 500, and the number of Pareto frontier non-dominated solution sets was 150. The 304 stainless steel process parameters turning were optimized by combining the DBO-BPNN and IPSO.

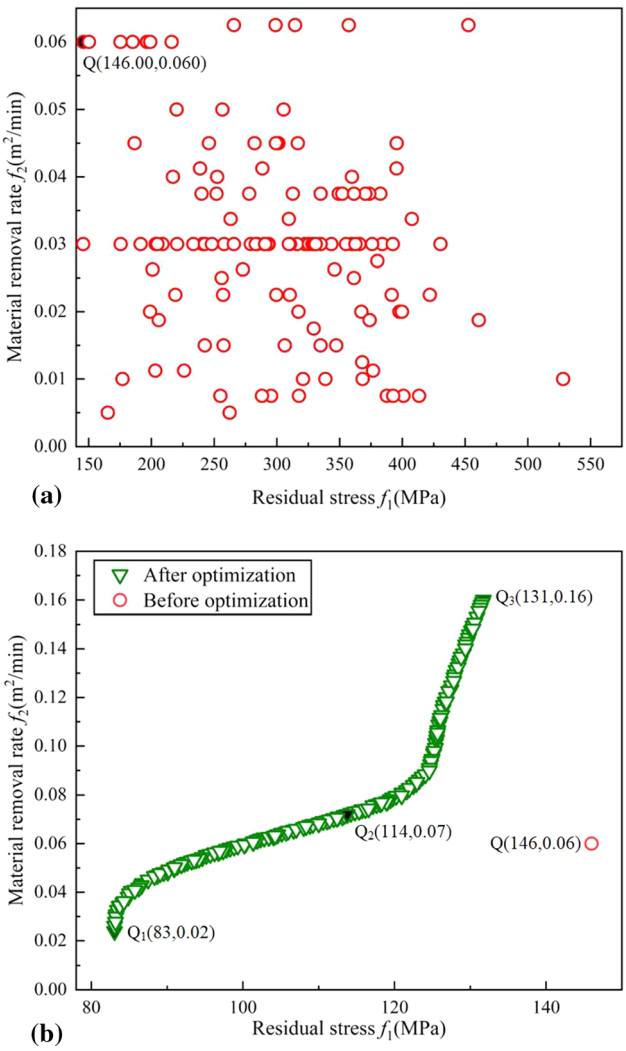

Fig. 12 Pareto optimal solution set, (a) Before optimization, (b) After optimization

The material removal rate and surface residual stress in CD solution set before optimization are shown in Fig. 12(a). Q was the optimal result of surface residual stress in CD and material removal rate that can be obtained from turning simulation.

Figure 12 (b) shows the optimization results. There are 150 solutions in the Pareto frontier solution set, representing Pareto optimal solutions of surface residual stress in CD and material removal rate under different weights. Q_1, Q_2 and Q_3 were the material removal rate and surface residual stress in CD after optimization. When the α_1=1, the optimization result for Q_1 (83,0.02). It was transformed into optimization with minimum surface residual stress in CD as a single objective. When the α_2=1, the optimization result for Q_3 (131,0.16). It was transformed into optimization with a maximum material removal rate as a single objective. When α_1= α_2=0.5, the optimization result for Q_2 (114,0.07). The optimization objective was both minimum surface residual stress in CD and maximum material removal rate.

The surface residual stresses in CD of Q_1, Q_2 and Q_3 were 83 MPa, 114 MPa and 131 MPa, respectively. The minimum surface residual stress in CD of the simulation was 146 MPa. They were 75.90, 28.07, and 11.45% lower than before optimization. The material removal rate of Q_2 and Q_3 were 0.07 m^2/min and 0.16 m^2/min, respectively. The simulated best material removal rate was 0.06m^2/min. Q_2 and Q_3 increased by 16.67 and 166.67% respectively compared to before optimization. The surface residual stress in CD was effectively reduced, and the material removal rate was improved.

The optimal turning process parameters of 304 stainless steel under different weight coefficients were obtained by decoding, as shown in Table 10.

In this paper, there was good consistency between the residual stresses on the surface of the 304 stainless steels obtained from the turning experiments and the FEM simulations. The established DBO-BPNN surface residual stress in CD prediction model had a prediction error of 4.77% and was able to accurately establish the nonlinear mapping relationship between turning parameters and surface residual stress in CD. Therefore, based on this mapping relationship, IPSO can quickly identify the Pareto solution set of turning parameters that result in the minimum surface residual stress in CD. Output turning parameters based on surface residual stress in CD and material removal rate weighting coefficients. Due to the differing weights assigned to surface residual stress in CD and material removal rate, the Pareto frontier solution set exhibits varying trends. At the forefront of the Pareto solution set, the weight assigned to surface residual stress in CD was greater than the weight assigned to material removal rate.

Table 10 Optimal turning parameters under different weights

Weights	Turning speed *v*, m/min	Turning depth *h*, mm	Tool front angle *e*, °	Tool back angle *f*, °	Tool radius *r*, mm
$Q_1(\alpha_1 = 1)$	60	0.40	15	8	0.02
$Q_2(\alpha_1 = 0.5)$	180	0.40	15	10	0.02
$Q_3(\alpha_2 = 1)$	400	0.40	15	5	0.02

Consequently, both surface residual stress in CD and material removal rate were minimized to a significant extent. In the back end of the Pareto solution set, the reverse was true. In the middle of the Pareto solution set, the weights assigned to surface residual stress in CD and material removal rate were similar. It was within this region that the turning parameters can simultaneously achieve maximum material removal rate and minimum surface residual stress in CD.

5. Conclusion

In this paper, the IPSO algorithm was applied to optimize the surface residual stress in CD and material removal rate to get the Pareto solution set of the optimal turning parameters. DBO-BPNN was adopted to map the nonlinear relationship between turning parameters and surface residual stress in CD. Then, turning simulation was used to obtain the surface residual stress in CD under different turning parameters. Turning experiments were adopted to verify the accuracy of the turning simulation. The results of the study are as follows:

(1) The maximum error between the turning experiment and the turning simulation experiment in the turning speed direction for residual stress is 32 MPa, with an average absolute percentage error of 5.10%. This indicates that the turning simulation model can be used to obtain the residual stress in the turning speed direction under different parameters.
(2) The mean absolute percentage error of the predictions of the three surface residual stress in CD prediction models (BPNN, GA-BPNN and DBO-BPNN) were 15.17, 10.68 and 4.77%, respectively. The results indicate that DBO-BPNN has a higher prediction accuracy and can more reliably forecast the surface residual stresses in CD of 304 stainless steel.
(3) Surface residual stress in CD and material removal rate were optimized with the combination IPSO and DBP-BPNN. The optimized surface residual stress in CD was decreased by an average of 38.48% and the material removal rate was increased by an average of 91.69%. The optimized turning parameters gained provided a feasible solution to improve the service life and reduce the production cost of 304 stainless steel parts.

Acknowledgment

This work is supported by the National Natural Science Foundation of China (Grant No. 52205148), the China Postdoctoral Science Foundation (Grant No. 2023M731392), the Natural Science Foundation of Hubei Province of China (Grant No. 2023AFB928) and the Scientific Research Project of Hubei Provincial Department of Education (Grant No. Q20239404).

References

1. S. Pal, S.S. Bhadauria, and P. Kumar, Studies on Stress Corrosion Cracking of F304 Stainless Steel in Boiling Magnesium Chloride Solution, *J. Bio- Tribo-Corr.*, 2021, **7**(2), p 62.
2. A.H. Elsheikh, S. Shanmugan, T. Muthuramalingam, A.K. Thakur, F.A. Essa, A.M.M. Ibrahim, and A.O. Mosleh, A Comprehensive Review on Residual Stresses in Turning, *Adv. Manufact.*, 2021, **10**(2), p 287–312.
3. B.P. Van, and H.T. Viet, Application of Bat Algorithm for Improvement of Surface Integrity in Turning of AISI 304 Austenitic Stainless Steel, *J. Korean Soc. Precision Eng.*, 2021, **38**(4), p 237–244.
4. G.R. dos Santos Biasibetti, R.M. Nunes, L.C. de Cesaro Cavaler, G.V. Braga Lemos, A.d.S. Rocha, Turning parameters effects in residual stresses of AISI 1045 steel In: *Proceedings of the Institution of Mechanical Engineers Part b-Journal of Engineering Manufacture*, **235**(9), 1498-1506 (2021)
5. X.T. Deng, M. Cheng, S.H. Zhang, H.W. Song, and M.A. Taha, Residual Stresses and Martensite Transformation in AISI 304 Austenitic Stainless Steel, *Mater. Res. Exp.*, 2019, **6**(1), 016503
6. W. Zhang, H. Wu, S. Wang, Y. Hu, K. Fang, and X. Wang, Investigation of Stress Corrosion Cracking Initiation in Machined 304 Austenitic Stainless Steel in Magnesium Chloride Environment, *J. Mater. Eng. Perform.*, 2020, **29**(1), p 191–204.
7. C.M Smudde, C.R. D'Elia, C.W.S., Marchi, M.R. Hill, J.C. Gibeling, The Influence of Residual Stress on Fatigue Crack Growth Rates of Additively Manufactured Type 304L stainless steel, *Int J Fatigue*, **162**, (2022) (in English)
8. H. Yahyaoui, N. Ben Moussa, C. Braham, N. Ben Fredj, and H. Sidhom, Role of Machining Defects and Residual Stress on the AISI 304 Fatigue Crack Nucleation, *Fatigue Fract. Eng. Mater. Struct*, 2015, **38**(4), p 420–433.
9. V. Sharma and P.M. Pandey, Optimization of Machining and Vibration Parameters for Residual Stresses Minimization in Ultrasonic Assisted Turning of 4340 Hardened Steel, *Ultrasonics*, 2016, **70**, p 172–182.
10. M. Sedlacek, B. Podgornik, and S. Milanovic, A Modified Heat Treatment to Improve the Properties of Double-layer Cast Rolls, *Materiali in Tehnologije*, 2014, **48**(6), p 983–990.
11. M. Mia, P.R. Dey, M.S. Hossain, M.T. Arafat, M. Asaduzzaman, M.S. Ullah, and S.M.T. Zobaer, Taguchi S/N based optimization of machining parameters for surface roughness, tool wear and material removal rate in hard turning under MQL cutting condition, *Measurement*, 2018, **122**, p 380–391.
12. Y. Su, G.Y. Zhao, Y.G. Zhao, J.B. Meng, and C.X. Li, Multi-Objective Optimization of Cutting Parameters in Turning AISI 304 Austenitic Stainless Steel, *Metals-Basel*, 2020, **10**(2), p 217. (**(in English)**)
13. R.A. Mahdavinejad and S. Saeedy, Investigation of the influential parameters of machining of AISI 304 stainless steel, *Sadhana*, 2011, **36**(6), p 963–970.
14. V. Varghese, M.R. Ramesh, and D. Chakradhar, Experimental Investigation and Optimization of Machining Parameters for Sustainable Machining, *Mater. Manuf. Process*, 2018, **33**(16), p 1782–1792. (**(in English)**)
15. S.E. Mirmohammadsadeghi and H. Amirabadi, High-pressure jet-assisted turning of AISI 304: Experimental and multi-objective optimization approach, *P I Mech Eng E-J Pro*, 2018, **232**(6), p 734–750. (**(in English)**)
16. T. Zhou, L. He, J.X. Wu, F.L. Du, and Z.F. Zou, Prediction of Surface Roughness of 304 Stainless Steel and Multi-Objective Optimization of Cutting Parameters Based on GA-GBRT, *Appl Sci-Basel*, 2019, **9**(18), p 3684. (**(in English)**)
17. M.S. Alajmi and A.M. Almeshal, Prediction and Optimization of Surface Roughness in a Turning Process Using the ANFIS-QPSO Method, *Materials*, 2020, **13**(13), p 2986. (**(in English)**)
18. F. Jafarian, M. Taghipour, and H. Amirabadi, Application of Artificial Neural Network and Optimization Algorithms for Optimizing Surface Roughness Tool Life and Cutting Forces in Turning Operation, *J Mech Sci Technol*, 2013, **27**(5), p 1469–1477. (**(in English)**)
19. F. Wang, H. Zhang, and A.M. Zhou, A Particle Swarm Optimization Algorithm for Mixed-variable Optimization Problems, *Swarm Evol Comput*, 2021, **60**, p 100808. (**(in English)**)
20. M. Mohammadi, S. Golabi, and B. Amirsalari, Determining Optimum Butt-Welding Parameters of 304 Stainless-Steel Plates Using Finite Element Particle Swarm and Artificial Neural Network, *Ijst-T Mech Eng*, 2021, **45**(3), p 787–800. (**(in English)**)
21. H.G. Zhou, W.B. Yang, L. Sun, X.W. Jing, G.C. Li, L.P. Cao, Reliability Optimization of Process Parameters for Marine Diesel Engine Block Hole System Machining using Improved PSO, *Sci Rep-Uk*, **11**(1), (2021) (in English)

22. X.F. Zhang, R. Liu, J.X. Ren, and Q.L. Gui, Adaptive Fractional Image Enhancement Algorithm Based on Rough Set and Particle Swarm Optimization, *Fractal Fract*, 2022, **6**(2), p 100. (**(in English)**)
23. M. Azadi Moghaddam, R. Golmezerji, and F. Kolahan, Simultaneous Optimization of Joint Edge Geometry and Process Parameters in Gas Metal Arc Welding using Integrated ANN-PSO Approach, *Sci. Iran.*, 2017, **24**(1), p 260–273. (**(in English)**)
24. P. Kahhal, M. Ghasemi, M. Kashfi, H. Ghorbani-Menghari, J.H. Kim, A Multi-objective Optimization using Response Surface Model Coupled with Particle Swarm Algorithm on FSW Process Parameters, *Sci Rep-Uk*, **12**(1), (2022) (in English)
25. E. Capello, Residual Stresses in Turning: Part I: Influence of Process Parameters, *J. Mater. Process. Technol.*, 2005, **160**(2), p 221–228.
26. R. dos Santos Pereira, R. Droppa, M.C. Lopes de Oliveira and R.A. Antunes, Effect of Milling Parameters on the Stability of the Passive Film of AISI 304 Stainless Steel, *J. Mater. Eng. Performan.*, 2021, **30**, p 8131–8144. (**(in English)**)
27. Y.Y. Chang, T. Sun and H.C. Wang, Experimental and FEM Study of Residual Stresses During Ultra-Precision Turning of Aluminum 2024–T3, *Exp. Tech.*, 2018, **42**(2), p 223–231.
28. J. Xue and B. Shen, Dung beetle Optimizer: a New Meta-heuristic Algorithm for Global Optimization, *J. Supercomput.*, 2023, **79**(7), p 7305–7336. (**(in English)**)
29. J. Huang and L. He, Application of Improved PSO - BP Neural Network in Customer Churn Warning, *Proc. Comput. Sci.*, 2018, **131**, p 1238–1246.
30. S. Katoch, S.S. Chauhan, and V. Kumar, A Review on Genetic Algorithm: Past, Present, and Future, *Multimed. Tools Appl.*, 2021, **80**(5), p 8091–8126.
31. W. Zhang, X. Wang, Y. Hu, and S. Wang, Predictive Modelling of Microstructure Changes, Micro-hardness and Residual Stress in Machining of 304 Austenitic Stainless Steel, *Int. J. Mach. Tools Manuf*, 2018, **130–131**, p 36–48.